Available online at www.sciencedirect.com
ScienceDirect
Journal of Asian Earth Sciences 29 (2007) 859–877
Journal of Asian Earth Sciences
www.elsevier.com/locate/jaes

Petrology and geochemistry of the granitoid complex of Boroujerd, Sanandaj-Sirjan Zone, Western Iran

A. Ahmadi Khalaji, D. Esmaeily *, M.V. Valizadeh, H. Rahimpour-Bonab

School of Geology, University College of Science, University of Tehran, Tehran, Iran

Received 19 May 2005; accepted 21 June 2006

Abstract

The Middle Jurassic Boroujerd Granitoid Complex of the Sanandaj-Sirjan Zone (with a U–Pb zircon age of 169–172 Ma) was emplaced in an active continental margin setting. This complex consists of three main units: an elongate NW–SE extending granodioritic unit ($SiO_2 = 58$–71 wt%), which is widespread throughout the area, a quartz-dioritic unit ($SiO_2 = 52$–63 wt%), exposed as small stocks within the granodioritic body, and a monzogranitic unit ($SiO_2 = 70$–75 wt%), widely scattered as separate small outcrops through the southern part of the area. A series of NW trending aplites and pegmatites are present in the granodioritic unit and its aureole.

Geochemically this complex is metaluminous to slightly peraluminous, typical of I-type granites. It belongs to high-K calc-alkaline series and displays the geochemical characteristics typical of volcanic arc granites related to an active continental margin (e.g. significant Nb, Ti, P and Sr depletion). Isotopic data ($Sr_i = 0.7062$–0.7074 and $\varepsilon Nd_t = -3.02$ to -3.62) are consistent with a crustal protolith. In addition, fractional crystallization may have played an important role in the formation of the whole spectrum of the granitoid types that occur in the Boroujerd area.

Keywords: Iran; I-type granite; Volcanic arc; Jurassic; Sanandaj-Sirjan

1. Introduction

Subduction of the Tethyan oceanic lithosphere under the southwestern border of Central Iran, caused plutonic and volcanic activity between the Jurassic and Quaternary within and adjacent to the Sanandaj-Sirjan Zone in the Northwest–Southeast of Iran (Figs. 1 and 2) (Ricou et al., 1977; Berberian and King, 1981; Berberian, 1983; Mohajjel et al., 2003).

The tectonic history of the Tethyan region has been studied by many authors (e.g. Takin, 1972; Stöcklin, 1974, 1977; Farhoudi, 1978; Berberian, 1981a,b; Berberian and King, 1981; Berberian and Berberian, 1981; Berberian et al., 1982; Jankovic, 1984; Sengör, 1984, 1990, 1991; Sengör et al., 1988; Shahabpour and Kramers, 1987;Alavi, 1994; among others). From Late Precambrian until Late Paleozoic time, southeastern Turkey, Central Iran, central Afghanistan, southern Pamir and Arabia were part of Gondwana, separated from the Eurasian Plate by Paleotethys. In the Middle to Late Triassic, during the closure of the Paleotethys in the north, rifting in the continental plate along the Zagros thrust zone occurred, which resulted in the opening of a new ocean, the Neotethys. During Triassic–Jurassic time following the closure of Paleotethys, the oceanic crust of the Neotethys started to subduct beneath the Eurasian Plate. This led to an Early Cimmerian metamorphic event, recorded in the southwest Sanandaj-Sirjan Zone (Berberian and King, 1981; Berberian and Berberian, 1981; Hooper et al., 1994) associated with the emplacement of intrusive bodies (Sabzehei, 1994; Berberian and Berberian, 1981) within this zone in the Upper Triassic. Finally, closure of Neotethys and collision of Arabia and Central Iran took place during Neogene time (Berberian and Berberian, 1981).

* Corresponding author. Tel.: +98 21 44443978; fax: +98 21 66405141.
E-mail address: esmaili@khayam.ut.ac.ir (D. Esmaeily).

1367-9120/$ - see front matter © 2006 Elsevier Ltd. All rights reserved.
doi:10.1016/j.jseaes.2006.06.005

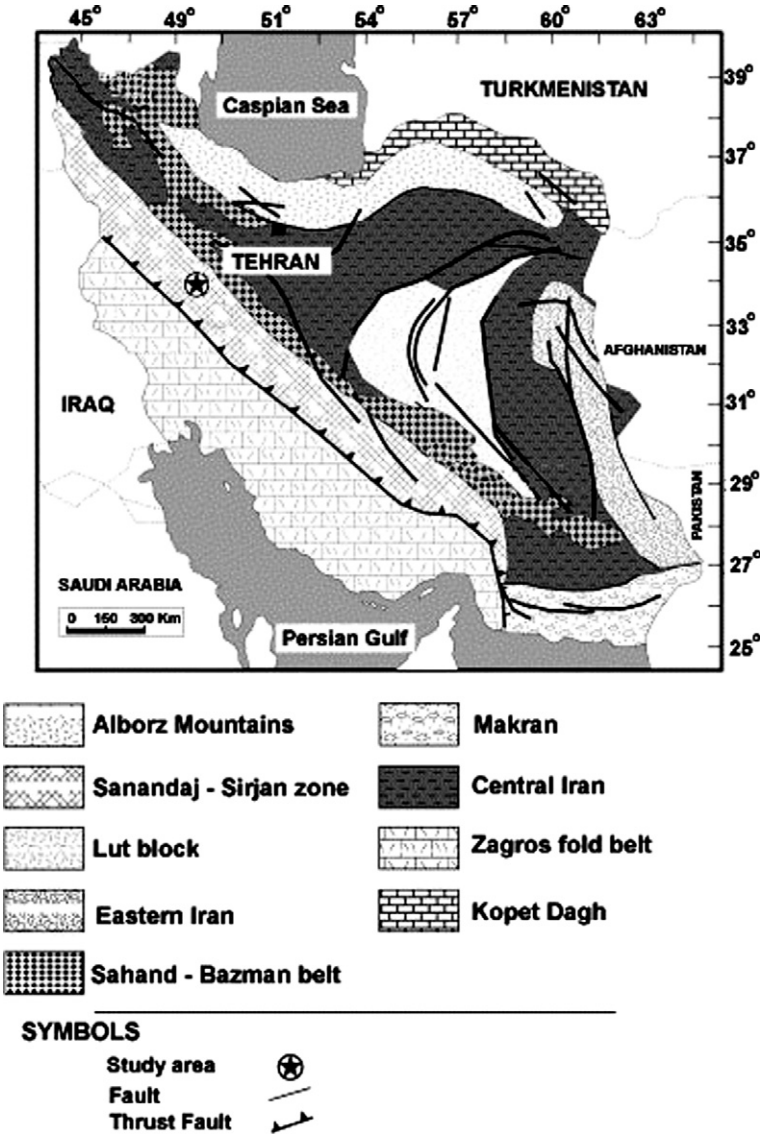

Fig. 1. Geological map of Iran (modified from: Stöcklin and Setudinia, 1972) showing major lithotectonic units.

The geological map of Iran (Fig. 1, modified from Stöcklin and Setudinia, 1972; Shahabpour, 1994) shows the following major lithotectonic units: (1) Zagros fold belt; (2) Sanandaj-Sirjan Zone (SSZ); (3) Central Iran Zone; (4) Sahand–Bazman Zone; (5) Lut Block; (6) Alborz and Kopeh Dagh zones; and (7) Eastern Iran and Makran zones.

The Sanandaj-Sirjan Zone, which is the host of the Boroujerd Granitoid Complex, has a length of 1500 km and a width up to 200 km, extending from the northwest to southeast of Iran (Fig. 2). This tectonic zone is mainly composed of Mesozoic and some Paleozoic rocks (Berberian, 1977) separating the stable Central Iran Block, from the Afro-Arabian Plate (Stöcklin, 1968). The metamorphosed and complexly deformed rocks include extensive areas of Mesozoic volcanic rocks, which are associated with abundant deformed and undeformed plutons. During most of the second half of the Mesozoic era, the Sanandaj-Sirjan Zone represented an active Andean-like continental margin in which calc-alkaline magmatic activity progressively shifted northwards (Berberian and King, 1981; Sengör, 1990). Today, it behaves as a fairly rigid block moving northwards at 14 mm/year with respect to stable Eurasia (Vernant et al., 2004).

The tectonic evolution of the Sanandaj-Sirjan Zone is show in the Table 1 and Fig. 3.

1. Rifting of the northeastern margin of the Arabia to form the southern arm of the Tethyan Ocean occurred in two events (Fig. 3a and b): the southern arm of Tethys Ocean formed by sea-floor spreading in the Late Permian (Bechennec et al., 1990) (Fig. 3a). Formation of the ocean was predated by glaciation in the Late Carboniferous to Early Permian, followed by shallow marine to

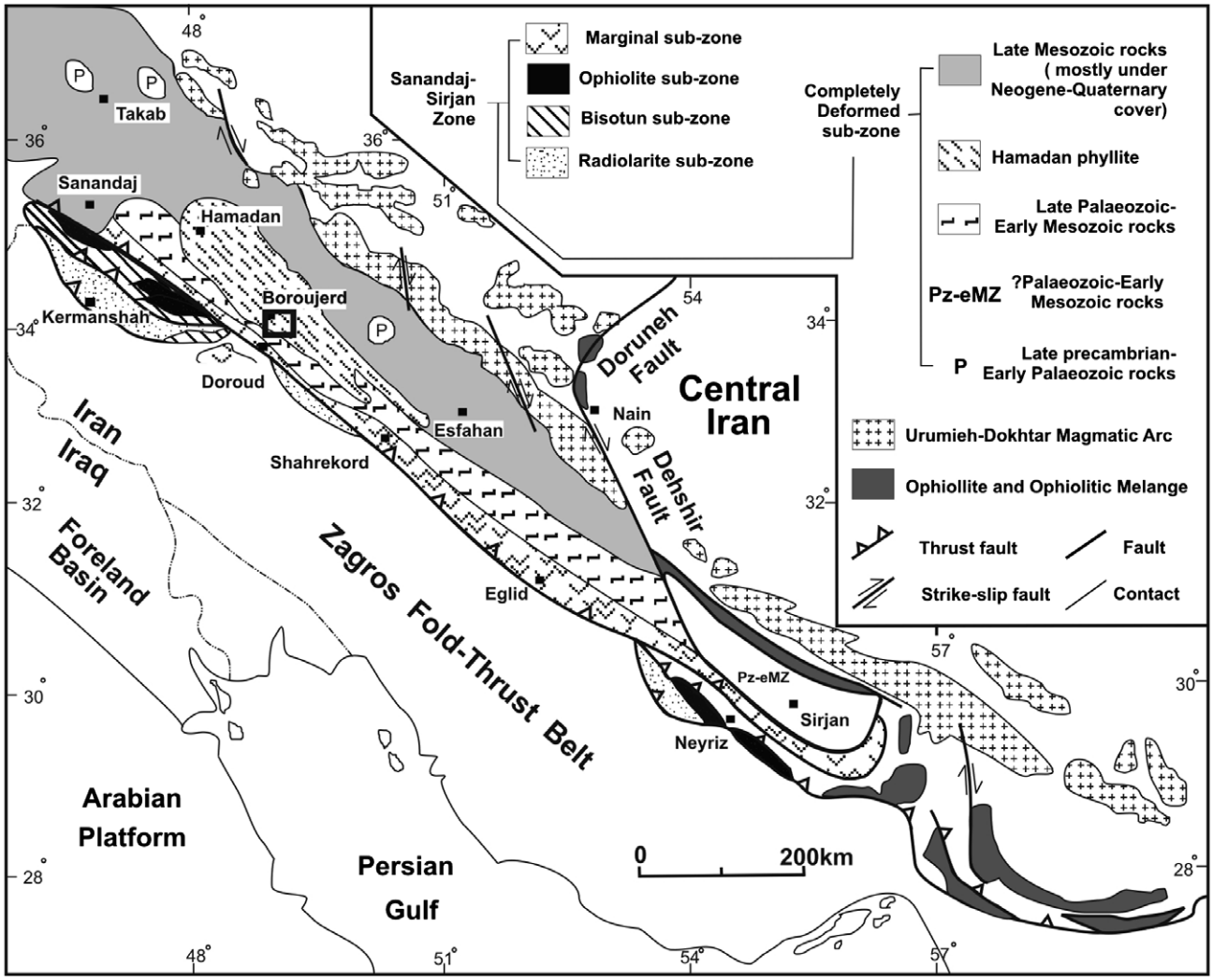

Fig. 2. Tectonic sketch map of western Iran (after Mohajjel et al., 2003) showing location of the Boroujerd Complex.

fluvial sedimentation in a Late Permian rim basin in Oman (Immenhauser et al., 2000); a Middle to Late Triassic extensional event that developed northwestwards as far as Turkey (Ricou, 1994) (Fig. 3b).

2. Generation of oceanic crust at about the Triassic–Jurassic boundary was accompanied by thermal contraction and subsidence of both passive margins. Renewed extension along both sides of the ocean in the late Triassic is shown by basaltic magmatic activity (June Complex) and widespread subsidence, with the deposition of the Hamadan Phyllite in the northeast and deep-marine sediments in the southwest (Fig. 3c). Subduction of Tethys to form a continental margin magmatic arc and associated plutonism, deformation and metamorphism.
3. Convergence was first accommodated by NE-ward subduction (with respect to the present geographic position) of the oceanic domain below the Iran Block (itself earlier accreted to Eurasia by the Late Triassic; Besse et al., 1998; Saidi et al., 1997) from the Late Triassic–Early Jurassic (Berberian and King, 1981; Davoudzadeh and Schmidt, 1984) or the Late Jurassic (Mohajjel and Fergusson, 2000). In the reconstructions of the Tethys by Sengör and Natal'in (1996) subduction is shown along the southern margin of the Podataksasi Zone, from the Middle Jurassic to the early Miocene. Igneous activity in the Boroujerd area is consistent with initiation of subduction at this time (Agard et al., 2005; their Fig. 12).
4. Ophiolite and related oceanic rocks were emplaced as an allochthon on the northeastern margin of Arabia. They were originally accreted to the northeastern margin of the Arabian Peninsula (i.e. the Zagros Fold-Thrust Belt) in the Late Cretaceous ophiolite obduction event. Ophiolite generation occurred at 80–95 Ma within Tethys and has been related by numerous authors to a mid-ocean ridge system in an overall convergent setting adjacent to a passive continental margin (e.g. Dercourt et al., 1986; Knipper et al., 1986; Hacker et al., 1996). Seemingly, in the Zagros, ophiolite obduction resulted from an island arc collision with the Arabian passive margin (Mohajjel et al., 2003).
5. Miocene collision of the northeastern margin of Arabia with Central Iran (Fig. 3f).

Table 1
The tectonic evolution of the Sanandaj-Sirjan Zone [modified (by our new data) from Mohajjel (1997), Mohajjel et al. (2003)]

Era	Period		Epoch	Tectonic events	Orogeny phase	Age (Ma)
Cenozoic	Tertiary	Neogene	Pliocene			
			Miocene	The continental collision between the Arabian and Central Iranian plates		
		Palegene	Oligocene			
			Eocene			
			Paleocene		Equivalent to Laramian phase	65
Mesozoic	Cretaceous		Upper	Ophiolite obduction		
			Lower		Late Cimmerian	135-140
	Jurassic		Upper			
			Middle	Compression tectonic (Subduction of Tethys to form a continental margin magmatic arc and associated plutonism	Middle Cimmerian	178
			Lower			
	Triassic		Upper			
			Middle	Extension tectonic (Rifting has started in the NW Gondwana margin)	Early Cimmerian	241.1
			Lower			
Paleozoic						

In this paper, we present new geochemical data including Sr–Nd isotopes on the granitoid plutons from the Boroujerd area of the Sanandaj-Sirjan Zone to constrain magma sources and evolution, to determine the tectonic setting of the Complex in the Sanandaj-Sirjan Zone and to shed light on this period of the Alpine history and related magmatism in Iran, an area for which little information has been available so far.

2. Geological setting and geochronology

The Boroujerd Complex (Fig. 4) is a NW–SE trending body covering an area of 600 km^2, approximately 60 km in length and 8–10 km in width, which lies between 33°38′–34°N and 48°45′–49°20′E. Detailed geological data from the area under study are scarce and are mainly reconnaissance reports. The Sanandaj-Sirjan Zone in the Boroujerd area is characterized by the predominance of metamorphic rocks and the presence of granitoids. The metamorphic rocks are composed of various metasedimentary assemblages of the low to high metamorphic grade. The basement of the area (Fig. 4) is composed of the pre-Jurassic, low- to very low-grade metamorphic rocks (June Complex, Mohajjel, 1997), such as meta-volcanic and tuffs, meta-cherty limestone, metasandstone, slates and phyllites (Hamadan Phyllite, Fig. 4).

Contact metamorphic rocks, consisting of spotted schists, cordierite–andalusite and cordierite–sillimanite hornfelses, are evident only to the north of the pluton,

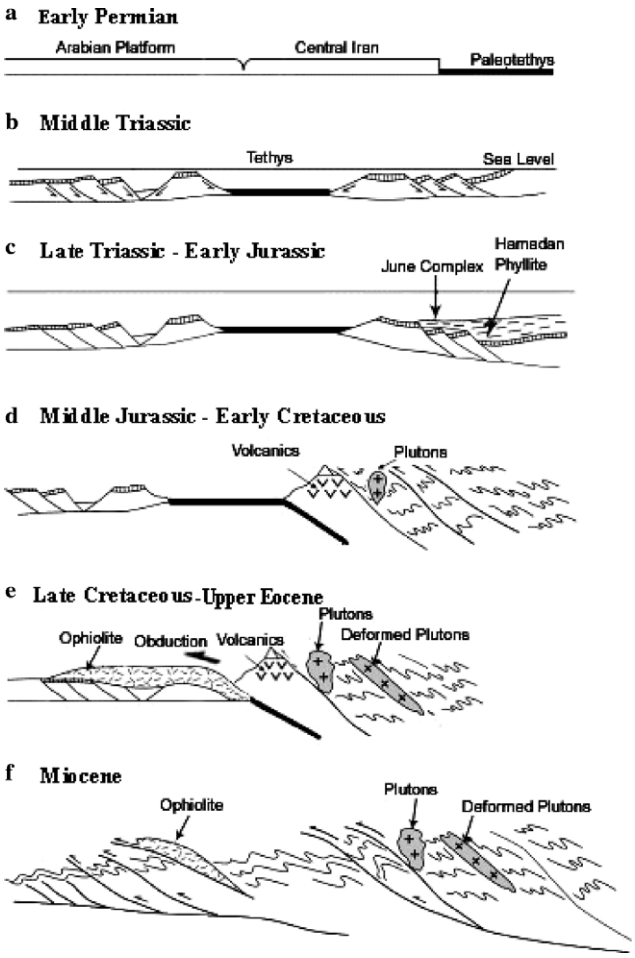

Fig. 3. Schematic cross-sections along the Zagros Orogen showing the tectonic evolution of the Sanandaj-Sirjan Zone [see text, modified (by our new data) from Mohajjel, 1997; Mohajjel et al., 2003].

because the southern margin of the complex is controlled by a fault system parallel to the contact where granitoid rocks are thrust over metamorphic rocks (Berthier et al., 1974; Masoudi, 1997).

New U–Pb zircon geochronological data from a variety of granitoid rocks, including the main units and associated pegmatitic dikes, indicate a strange, but short-lived episode of magmatic activity during the period of 169 Ma to 172 Ma in the middle Jurassic (Khalaji et al., 2005; Khalaji, 2006). They represent new precise U–Pb single zircon dating for six different granitoid samples, including three samples from the granodioritic unit (B1A55, G5 and AS2), one sample from the quartz-diorite unit (G12), the monzogranite unit (GM10) and a pegmatite dyke (B2A17) (Table 2). The analyses were carried out on a VG sector 354 mass spectrometer at the Massachusetts Institute of Technology, USA. Previously Masoudi (1997) and Masoudi et al. (2002) have ascribed an Early Cretaceous (about 120 Ma) to Late Cretaceous–Early Paleocene (70–52 Ma) age to these intrusions. The new isotopic data provide a new Middle Jurassic (169–172 Ma) age for these granitoid rocks.

3. Petrography

Detailed mapping of the Boroujerd Complex (Fig. 4) distinguished three main rock types, hereafter referred to as the granodioritic unit, quartz-dioritic unit and monzogranitic unit, locally associated with acidic dikes.

3.1. Granodioritic unit

The widespread granodioritic unit ranges in composition between tonalite to granodiorite and forms a large elongated NW-extending pluton (Fig. 4). It shows clear foliation due to the orientation of minerals, especially biotite. It also shows medium to coarse-grained textures with a simple mineralogy (Fig. 5a): plagioclase (30–40%), biotite (10–20%), quartz (25–30%) and alkali feldspar (<20%). Apatite, zircon, allanite and opaques are common accessory minerals and some muscovite is present as a secondary mineral. Plagioclase forms rectangular to subhedral plates, 2–3 mm or less in length that exhibit variable amounts of sericitisation. This mineral displays some zoning and, based on the textural relationships, it could be the first felsic mineral to crystallize. Biotite occurs as brown flakes, 2–3 mm in length, with a preferred orientation, but may be kinked due to deformation, and is mostly altered to chlorite and/or titanite, prehnite, muscovite and opaques. Quartz crystals occur as anhedral isolated grains and aggregates which display recrystallisation with undulatory extinction, typical of incipient solid-state deformation.

3.2. Quartz-diorite unit

Many small stocks of quartz-dioritic composition are exposed within the granodioritic body (Fig. 4). The contact between granodioritic and quartz-dioritic units is generally sharp. The grain size is not very variable, being 2 mm on average (Fig. 5b). These rocks have a granular to porphyritic texture with plagioclase megacrysts, and are composed predominantly of plagioclase (40–50%), biotite (15–20%), green amphibole (10–15%), quartz (<15%) and alkali feldspar (<5%). Plagioclase occurs as zoned euhedral to subhedral plates, 2–3 mm average size, and sometimes altered to sericite, epidote and calcite. Biotite occurs as brown kinked flakes, 1–3 mm in size, deformed and altered to chlorite, or an aggregate of sphene, prehnite, muscovite, opaques and quartz. Green amphibole forms subhedral to euhedral prismatic crystals, 1–3 mm long, and shows some alteration to biotite, chlorite, epidote and prehnite. Zircon, titanite and apatite are conspicuous accessory minerals.

3.3. Monzogranitic unit

The monzogranitic unit is widely scattered as separate and small outcrops through the southern part of the area

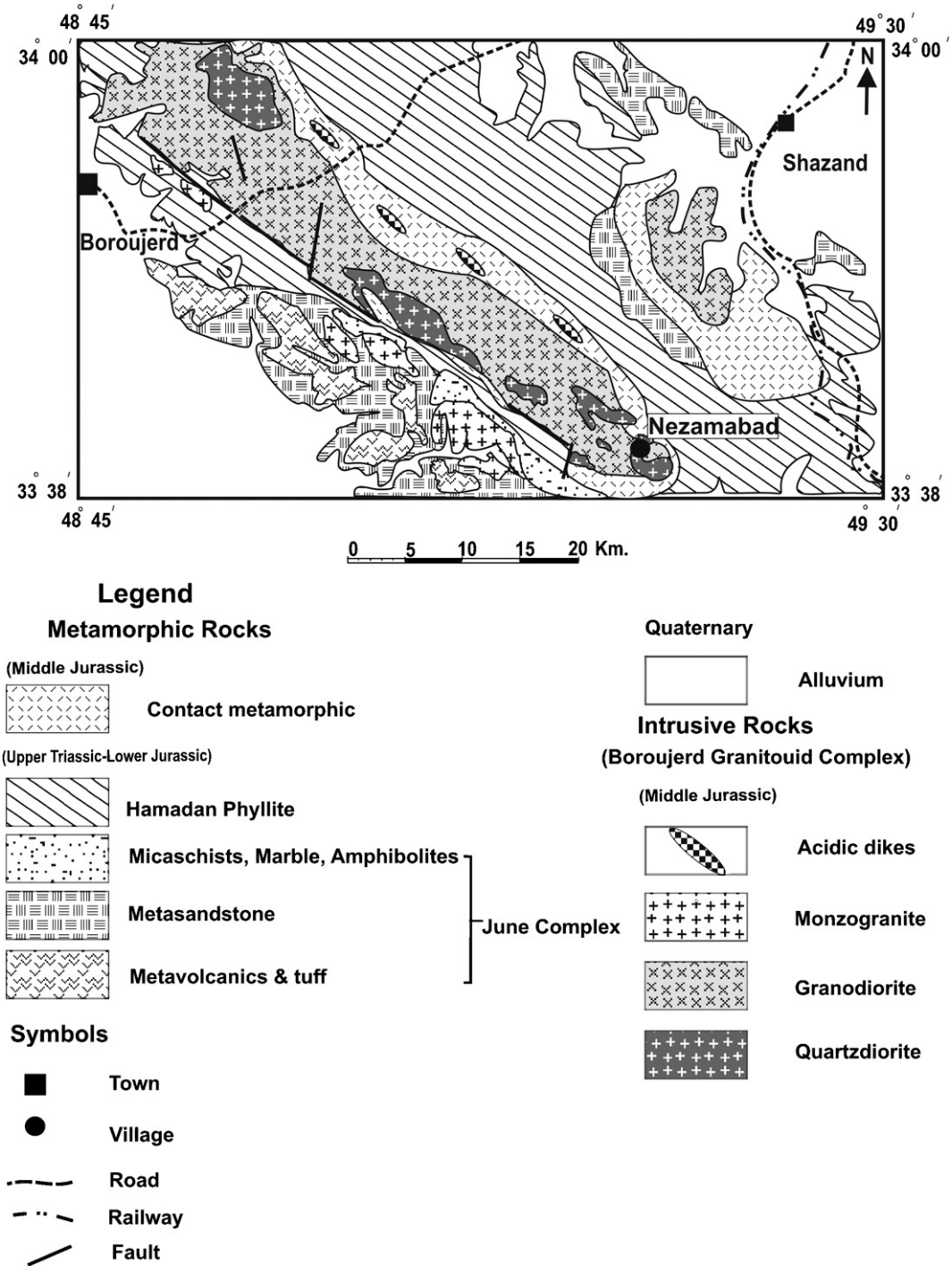

Fig. 4. Simplified geological map of the Boroujerd Granitoid Complex (Sohieili, 1992).

Table 2
New U–Pb zircon geochronologic data from a variety of granitoid rocks from the Boroujerd Granitoid Complex (Khalaji, 2006; Khalaji et al., 2005)

Sample	Lithology	Age (Ma)
G12	Quartz-diorite	170.7 ± 1.6
B1A55	Granodiorite	169.6 ± 0.2
G5	Granodiorite	171.3 ± 1.1
AS2	Granodiorite	170.7 ± 1
GM10	Monzogranite	171.7 ± 1.5
B2A17	Pegmatite	170.7 ± 1.5

(Fig. 4). These rocks are light in colour, fine to coarse-grained, with a granular texture (in the centre of the unit) and a porphyritic texture with feldspar megacrysts at the margin. Mineral assemblages include quartz (30–35%) alkali feldspar (30–35%), plagioclase (25–35%), biotite (5–10%) and some secondary muscovite. Zircon, allanite and apatite are common accessory minerals (Fig. 5c). Quartz intergrowths with K-feldspar and plagioclase form micrographic and/or granophyric textures and myrmekites, respectively. Large phenocrysts

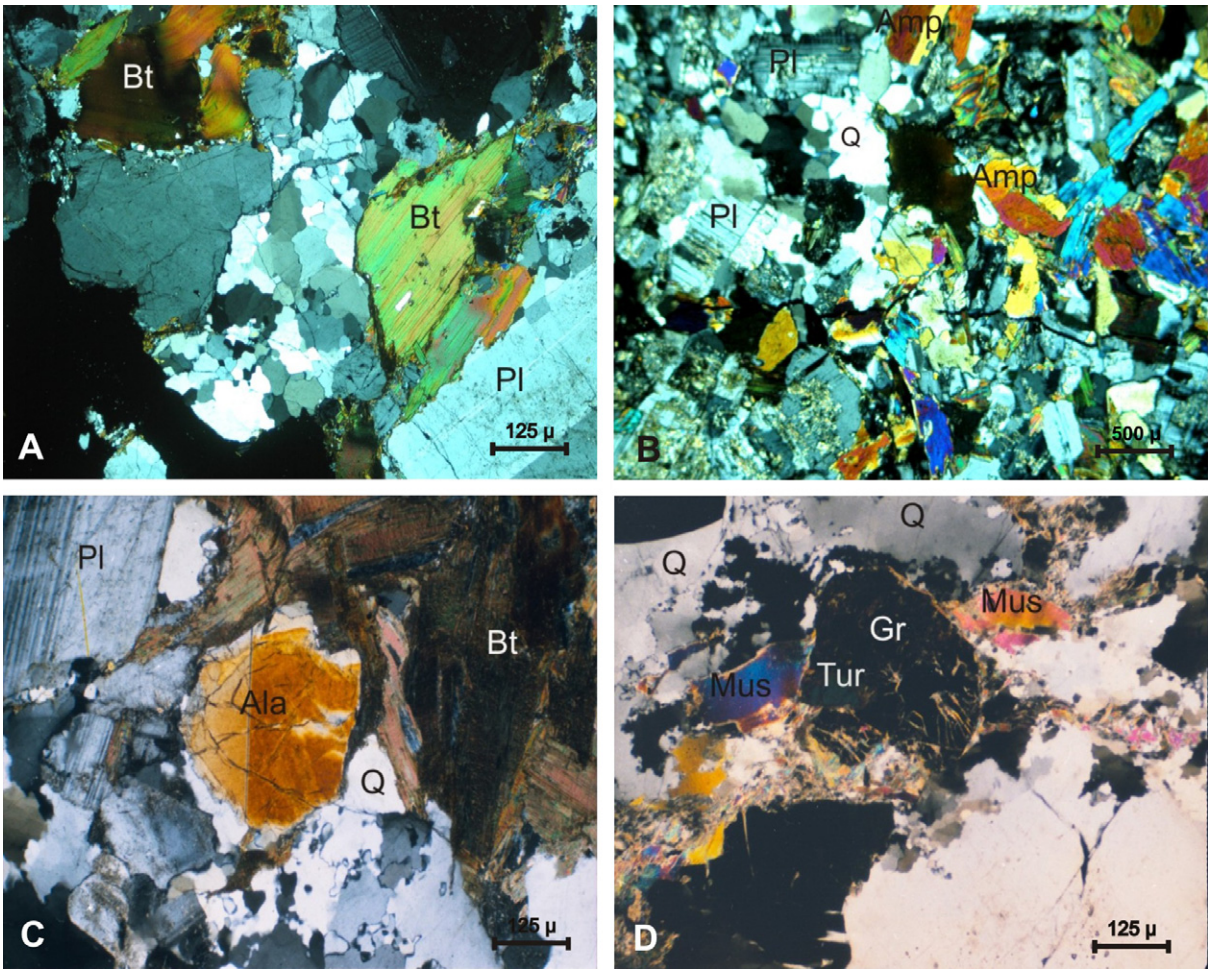

Fig. 5. Microphotographs of representative samples (crossed polarized light): (A) granodiorite; (B) quartz-diorite; (C) monzogranite; (D) pegmatite. Ala = allanite; Bt = biotite; Gr = garnet; Amp = amphibole; Mus = muscovite; Pl = plagioclase; Q = quartz; Tur = tourmaline.

of the quartz show undulatory extinction. Perthitic alkali-feldspar occurs as euhedral to subhedral crystals. Plagioclase is commonly zoned and again appears to be the first felsic mineral to crystallize.

3.4. Acidic dikes (aplites and pegmatites)

A series of NW trending aplites and pegmatites (Fig. 4), varying from a few meters to tens of meters in length and a few meters in width, occur in the area studied. The aplites are characterized by a fine equigranular assemblage of quartz, alkali-feldspar, some muscovite, tourmaline and opaque oxides. These rocks represent the final phase of magmatic activity. Pegmatites are mainly present in the granodioritic unit and its aureole. They show a simple mineralogy with graphic texture. They are characteristically composed of quartz, feldspar, muscovite, tourmaline, zircon and apatite, with some andalusite and garnet in the aureole samples (Fig. 5d). Pegmatites are similar in age to the main units and, again, could represent the final phase of magmatic activity.

4. Geochemistry

4.1. Sampling and analytical methods

A total of about three hundred rock samples from different localities, including the granodioritic unit, the quartz-dioritic unit, the monzogranitic unit, together with acidic dikes and enclaves were collected. Two hundred thin sections were studied by optical microscope. Thirty-one representative samples were then selected for whole rock chemical analysis (Table 3). Samples weighed between 1–1.5 kg before crushing and powdering. Major and trace element abundances were determined by inductively coupled plasma atomic emission spectrometry (ICP-AES) and inductively coupled plasma-mass spectrometry (ICP-MS) at the ALS Chemex laboratories in Vancouver, Canada. The analytical processes are described in Cotten et al. (1995). Relative standard deviations were ±2% for major elements and ±5% for trace elements. The results of these analyses are reported in Table 3.

Sr isotopic results were obtained using a Vg MM30 single-collector mass spectrometer at the Department of

Table 3
Major and trace element contents from the Boroujerd Granitoid Complex

Sample	Quartz-diorites										
	G14	G16	G18	G19	B2A31	GM25	G12	G11	AG2	B2A28	B2A33
SiO_2%	63.4	60.7	59.9	59.2	58.9	57.9	56.3	55.5	55.4	53.2	52.6
TiO_2	0.6	0.6	0.6	0.8	0.7	0.6	0.9	0.7	1.3	0.7	0.6
Al_2O_3	16.6	14.9	15.4	15.9	16.2	15.3	17.1	15.9	16.8	15.6	15.2
Fe_2O_3 t	6	6.4	6.6	7.1	7.1	6.9	8	7.8	8.6	8.7	8.7
MnO	0.1	0.1	0.1	0.1	0.1	0.1	0.2	0.2	0.2	0.2	0.2
MgO	3.3	4.3	4.6	4.8	4.7	6.5	5.1	6.5	4.6	7.6	8.4
CaO	5.6	5.2	5.6	5.5	5.9	6.1	6.9	6.4	7.3	7.8	8.9
Na_2O	1.4	2.2	2.3	2.4	2.5	2.4	2.5	2.5	2.7	2.3	1.9
K_2O	2.3	3.5	3	2.8	2	2.5	2.1	2.2	1.8	2.1	1.8
P_2O_5	0.2	0.1	0.1	0.2	0.1	0.1	0.2	0.1	0.3	0.1	0.1
Ni (ppm)	37	53	57	63	49	115	75	101	38	86	103
Cr	260	280	260	330	320	420	360	450	150	490	690
Co	20	20.3	20.6	22.9	23.8	48	27.8	28.7	54.5	31.9	36.4
V	176	144	144	148	150	170	204	210	168	217	274
Cs	9.9	6	6.2	7.5	4.7	10	5.4	4.6	4.2	3.2	3.5
Rb	103	128	105	111	77.4	106.5	88.2	101	66.6	78.8	65.9
Sr	299	263	269	261	231	347	347	388	334	197	202
Ba	242	596	388	372	361	407	355	454	296	236	238
Th	4	24	7	13	5	11	9	10	7	5	5
U	2.5	3	2	1.8	2.3	2.1	2.4	2.6	1.9	1.4	1.2
Ta	0.8	1	0.9	0.9	0.9	0.9	0.9	0.7	1.1	0.5	0.5
Nb	8	12	10	12	10	10	12	9	13	7	8
Hf	4	4	5	5	4	5	5	5	3	2	2
Zr	117	115	139	179.5	123.5	164	161.5	175.5	90	77.6	71.6
Zn	96	70	62	69	58	68	127	118	79	63	114
Ga	19	18	17	19	18	18	22	20	19	16	18
Sn	5	3	2	2	2	6	3	4	3	1	2
W	9	5	3	4	14	217	8	5	269	1	3
La	13.8	68.3	19.4	33.8	16.4	28.8	27.2	24.1	19	16.6	20
Ce	32.9	146.5	44.2	72.3	41.5	55.6	57.6	50.1	44.4	39.4	50.7
Pr	3.8	14.8	5.4	7.9	5.7	6.7	6.7	5.8	5.1	4.4	6.1
Nd	14.8	49.4	20.9	28.7	24	24	25	21.8	19.8	16.2	23.9
Sm	3.9	8.3	4.4	5.6	5.4	4.8	5	4.4	4.8	3.5	5
Eu	0.1	1.1	0.7	1.2	0.8	1.1	0.4	0.1	1.1	0.8	0.1
Gd	3.8	7.8	4.6	5.6	5.3	4.6	5.1	4.1	4.5	3.8	5.2
Tb	0.6	1	0.7	0.8	0.8	0.7	0.7	0.6	0.6	0.5	0.8
Dy	3.7	5.7	4.2	4.4	5.1	3.8	4.3	3.5	3.8	3.5	4.6
Ho	0.7	1.1	0.9	0.9	1	0.8	0.8	0.8	0.7	0.7	1
Er	2.1	3.4	2.6	2.6	3.2	2.3	2.6	2.2	2.1	2.1	2.9
Tm	0.3	0.5	0.4	0.4	0.5	0.3	0.4	0.3	0.3	0.3	0.4
Yb	1.9	3.4	2.5	2.6	3.2	2.3	2.5	2.2	2	2	2.8
Lu	0.3	0.5	0.4	0.4	0.5	0.3	0.4	0.3	0.3	0.3	0.4
Y	20.4	30.7	22.5	23.3	30.2	21.6	23.4	19.8	18.2	18.4	26.6
Eu/Eu^*	0.1	0.4	0.5	0.7	0.5	0.7	0.2	0.1	0.7	0.7	0
(La/Yb)N	4.9	13.4	5.2	8.7	3.4	8.4	7.3	7.3	6.4	5.6	4.8

Sample	Granodiorites											
	MA3[a]	AS2	GM5[a]	AGH1	G6	G4	G5	AGH6	B1A55	AD4	AKY13	B4A19
SiO_2%	71.4	70.6	67.2	64.9	64.3	63.8	63.4	62.8	60.6	59.7	58.5	57.8
TiO_2	0.3	0.3	0.5	0.5	0.6	0.6	0.6	0.7	0.7	0.6	1	1
Al_2O_3	14.7	14.5	15.5	16	16.7	16.9	16.1	16.9	17.5	20.2	18	18.3
Fe_2O_3 t	1	3.5	2	4.5	5.5	5.6	5.2	5.7	6.5	4.3	8	8.7
MnO	0	0.1	0	0.1	0.1	0.1	0.1	0.1	0.1	0	0.1	0.1
MgO	2.9	0.9	3.9	1.4	1.6	1.6	1.5	1.8	1.8	1.3	2.4	2.5
CaO	0.3	2.2	0.7	2.5	3.9	3.8	3.8	3.8	4.1	5.2	4.1	4.3
Na_2O	4.8	3	4.2	3.1	3.1	3	2.9	3.4	2.9	3.6	2.5	2.6
K_2O	1.3	4.1	1.4	4	3.4	3.6	3.4	3	3.4	3.4	3.2	3.3
P_2O_5	0.1	0.1	0.2	0.1	0.2	0.1	0.1	0.2	0.3	0.2	0.4	0.1
Ni (ppm)	12	13	18	18	17	16	19	21	22	10	32	47
Cr	20	120	40	150	120	120	90	110	150	100	180	160
Co	55.3	6.4	41.9	10.2	12	11.1	11.1	11.8	12.8	8.9	18.6	19.6
V	31	36	55	60	88	88	81	78	97	50	155	152

Table 3 (*continued*)

Sample	Granodiorites											
	MA3[a]	AS2	GM5[a]	AGH1	G6	G4	G5	AGH6	B1A55	AD4	AKY13	B4A19
Cs	0.5	5.2	0.9	9.3	3.8	3.5	3	4.5	5.8	4.3	4.1	4.7
Rb	40.8	142.5	29.3	146	130.5	133.5	122	111	134.5	133.5	129.5	142.5
Sr	26.9	200	65.9	256	322	319	295	320	338	484	294	330
Ba	80.2	441	172.5	577	598	596	551	549	765	1150	763	853
Th	23	24	23	21	12	10	17	32	2	14	15	25
U	2.2	2.7	1.6	1.9	2.4	3.3	2.5	2.3	1.4	2.3	1.9	2.2
Ta	1.5	1.1	1.2	1	0.9	1	0.9	1	0.9	0.8	0.9	1
Nb	13	12	16	14	14	13	14	17	15	15	19	21
Hf	5	5	6	5	6	6	6	7	6	9	8	9
Zr	147.5	162.5	210	179.5	203	203	198.5	227	232	341	274	287
Zn	10	27	18	43	56	52	51	48	58	53	83	124
Ga	15	17	15	21	22	20	21	20	20	25	22	26
Sn	2	2	2	2	1	1	1	1	2	2	1	2
W	550	5	420	15	6	9	4	7	8	5	10	5
La	52.3	48.7	28.6	47.3	29.4	44.2	40.7	62.1	19.5	64	51	76.4
Ce	94.1	93.6	52.2	91.1	59.9	92.6	82.5	104.5	40.8	118.5	103	155
Pr	10.6	10	6	9.6	6.4	9.3	8.6	11.8	4.1	11.6	11	16.2
Nd	35.8	33.1	21.2	32.3	22.4	31	30	40.9	15.1	38.8	39.2	56.6
Sm	6.3	6.6	3.9	5.3	4	4.8	5.2	5.9	2.3	6.2	7	9.4
Eu	0.6	1.2	0.2	1.2	1	1.1	0.9	0.9	1.3	2.2	1.3	0.8
Gd	5.7	6.6	3.7	6	4.1	4.3	4.7	5.9	2.2	6.3	6.8	8.3
Tb	0.8	0.8	0.5	0.7	0.5	0.6	0.6	0.6	0.2	0.8	0.9	1
Dy	4.5	5.1	2.7	3.8	2.9	3.4	3.6	3	1.1	3.6	5.3	6.3
Ho	0.9	1	0.6	0.7	0.6	0.7	0.7	0.6	0.2	0.5	1.1	1.4
Er	2.8	3.1	1.6	2	2.1	2.1	2	1.6	0.7	1.2	3.6	4.5
Tm	0.4	0.4	0.2	0.2	0.3	0.3	0.3	0.2	0.1	0.1	0.5	0.6
Yb	2.7	2.9	1.5	1.7	2	2.3	1.8	1.4	0.7	0.8	3.4	4.5
Lu	0.4	0.4	0.2	0.2	0.3	0.4	0.3	0.2	0.1	0.1	0.5	0.6
Y	27.8	27.2	15.2	19.2	18.8	20.2	19.6	13.8	6.7	15	31.6	37.4
Eu/Eu*	0.3	0.6	0.2	0.7	0.8	0.7	0.6	0.5	1.8	1.1	0.6	0.3
(La/Yb)N	13	11.2	12.7	18.6	9.8	12.9	15.1	29.7	18.6	53.5	10	11.4

Sample	Monzogranites							
	G22[a]	AG19	GM11	AB6[a]	AG18	G24	GM10	G23
SiO_2%	75.1	73.7	71.4	71.1	70.8	70.7	70	69.7
TiO_2	0.1	0.3	0.3	0.2	0.4	0.2	0.3	0.2
Al_2O_3	12.8	12.8	14	14.5	13.5	14.6	14.1	14.9
Fe_2O_3 t	1.1	2.2	3	2	2.8	2.2	3.5	2.5
MnO	0	0.1	0.1	0	0.1	0.1	0.1	0.1
MgO	0.1	0.4	0.6	1.2	0.6	0.4	0.7	0.5
CaO	0.5	0.9	1.8	0.9	1	1.7	2.1	1.8
Na_2O	3.7	3.8	3	4.2	3.9	3.8	2.8	4.1
K_2O	4.6	3.8	4.1	2.1	4.1	4.6	4	4.2
P_2O_5	0	0.1	0.1	0.1	0.1	0	0.1	0
Ni (ppm)	7	7	11	13	20	9	12	8
Cr	130	10	20	150	10	80	20	110
Co	1.2	54.1	32.9	3.3	54.7	3.7	53.4	3.5
V	3.3	17	24	23	27	11	29	11
Cs	3.7	0.8	2.7	2.3	1.1	4.5	6.2	4.5
Rb	189	129	146.5	63.8	123.5	157	166.5	152.5
Sr	27.8	121.5	229	114	168	124.5	239	132.5
Ba	38.5	320	399	276	631	408	404	372
Th	19	31	15	16	32	11	20	13
U	3.8	5.8	2.6	2.5	5.3	2.4	2.7	2.6
Ta	1.5	3.2	1.4	1.1	2.6	0.9	1.4	1.1
Nb	9	32	11	10	28	10	11	11
Hf	4	5	4	4	6	4	4	5
Zr	81.5	178	116.5	106	230	128	137	149
Zn	16	30	29	13	79	39	35	47
Ga	16	19	17	17	20	17	17	17
Sn	3	3	2	3	4	4	2	4
W	8	469	225	8	416	11	429	11

La	7.3	42.7	32.9	32.5	59.5	20.1	39.7	25.1

(continued on next page)

Table 3 (*continued*)

Sample	Monzogranites							
	G22[a]	AG19	GM11	AB6[a]	AG18	G24	GM10	G23
Ce	18	74.6	64.6	64.1	101.5	40.5	77.4	54.5
Pr	2.4	7.2	6.9	6.5	9.7	4.2	8.3	5.6
Nd	9.8	23	23.7	22.3	29.6	15	28.7	20.3
Sm	4	4.5	4.5	4.5	5.2	3.3	5.2	4.4
Eu	0.1	0.9	0.7	0.7	0.1	0.4	0.5	0.2
Gd	5.7	4.6	4.1	4.2	5.3	3.6	5.1	4.2
Tb	1.2	0.7	0.6	0.6	0.7	0.6	0.7	0.6
Dy	8.8	4.2	3.5	3.7	4	3.5	3.9	4.1
Ho	2	0.8	0.7	0.7	0.8	0.7	0.8	0.8
Er	6	2.5	1.9	2.2	2.5	2.1	2.2	2.7
Tm	1	0.4	0.3	0.3	0.4	0.3	0.3	0.4
Yb	6.6	2.9	2	2.4	2.6	2.1	2.2	2.6
Lu	0.9	0.4	0.3	0.3	0.4	0.3	0.3	0.4
Y	59.5	22.8	19.2	20.2	22.8	20.3	21	23.3

Line missing

Earth, Atmospheric and Planetary Science, MIT (Cambridge, Massachusetts, USA). Sr, loaded on single Re filaments, was analyzed in dynamic multi-collector mode with $^{88}Sr = 3$ V. All Sr data are normalized to $^{86}Sr/^{88}Sr = 0.1194$ and analytical uncertainty for $^{86}Sr/^{88}Sr$ is 1 in the fifth decimal place or better (2σ). Long term reproducibility of NBS-987 standard at MIT is 0.710247 ± 0.000014 (2σ).

Nd isotope ratios were obtained using a VG 354 Five-collector mass spectrometer at MIT. $^{143}Nd/^{144}Nd$ ratios were corrected for fractionation relative to $^{143}Nd/^{144}Nd = 0.7219$. Replicate runs for the La Jolla Nd standard gave $^{143}Nd/^{144}Nd$ values that were normalized relative to 0.511855, matching the accepted value for the La Jolla standard (Wasserburg et al., 1981). Dissolution and chemical separation techniques and mass spectrometer procedures for whole-rock Sr and Nd isotope analyses have been reported by Tronnes and Brandon (1992). The results of the Sr and Nd isotope analyses are reported in Table 4.

4.2. Major elements

SiO_2 contents of different samples exhibit wide ranges, from approximately 52–63 wt% for the quartz-dioritic unit, 58–71 wt% for the granodioritic unit and 70–75 wt% for the monzogranitic unit (Table 3). Major and trace element variations are illustrated in Harker diagrams (Figs. 6 and 7). Most of the samples display near-linear to curvilinear trends of decreasing Al_2O_3, TiO_2, Fe_2O_3, MgO, MnO, CaO and P_2O_5 and increasing K_2O and Na_2O with increasing SiO_2 content.

Harker diagrams of the major elements (Fig. 6) have trends suggesting clearly that the granodioritic and monzogranitic units may be co-magmatic, whereas the quartz-diorites seems to be derived from a different source or by

Table 4
Sm–Nd and Rb–Sr isotopic data from the Boroujerd Granitoid Complex

Sample	G12	B2A31	AD4	B1A55	GM10
Rock type	QZ diorite	QZ diorite	Granodiorite	Granodiorite	Monzogranite
Rb (ppm)	88.2	77.4	133.5	134.5	166.5
Sr (ppm)	347	231	484	338	239
$^{87}Rb/^{86}Sr$	0.73535	0.96953	0.79803	1.1514	2.161
$^{87}Sr/^{86}Sr$ (a)	0.70795	0.70976	0.70856	0.70936	0.71114
$^{87}Sr/^{86}Sr_{(i)}$	0.7062	0.7074	0.7066	0.7066	0.7063
Sm (ppm)	4.84	5.59	7.74	7.72	5.97
Nd (ppm)	23.73	24.5	52.75	51.15	31.47
$^{147}Sm/^{144}Nd$	0.12337	0.13804	0.08874	0.09129	0.11478
$^{143}Nd/^{144}Nd$	0.51237	0.51241	0.51234	0.51235	0.51239
$(^{143}Nd/^{144}Nd)_i$	0.51223	0.51226	0.51224	0.51225	0.51226
$\varepsilon Nd_{(0)}$	−5.22	−4.41	−5.88	−5.62	−4.8
$\varepsilon Nd_{(\tau)}$	−3.62	−3.14	−3.53	−3.33	−3.02
T(DM)	1135	1269	867	869	1006
$f_{Sm/Nd}$	−0.37	−0.3	−0.55	−0.54	−0.42

Nd isotopic normalized to $^{146}Nd/^{144}Nd = 0.7219$. εNd calculated at $T = 170$ Ma for rocks. (a) Long term reproducibility of NBS-987 standard at MIT: 0.710240 ± 000014 (2σ SD). $\varepsilon(T) = [Rm(T)/RCHUR(T) - 1] \times 104$, where $Rm(T)$ and $RCHUR(T)$ refer to the isotopic ratios of $^{143}Nd/^{144}Nd$ for a sample (m) and CHUR, $(^{143}Nd/^{144}Nd)$ CHUR(0) = 0.512638 and $(^{147}Sm/^{144}Nd)$ CHUR(0) = 0.1967.

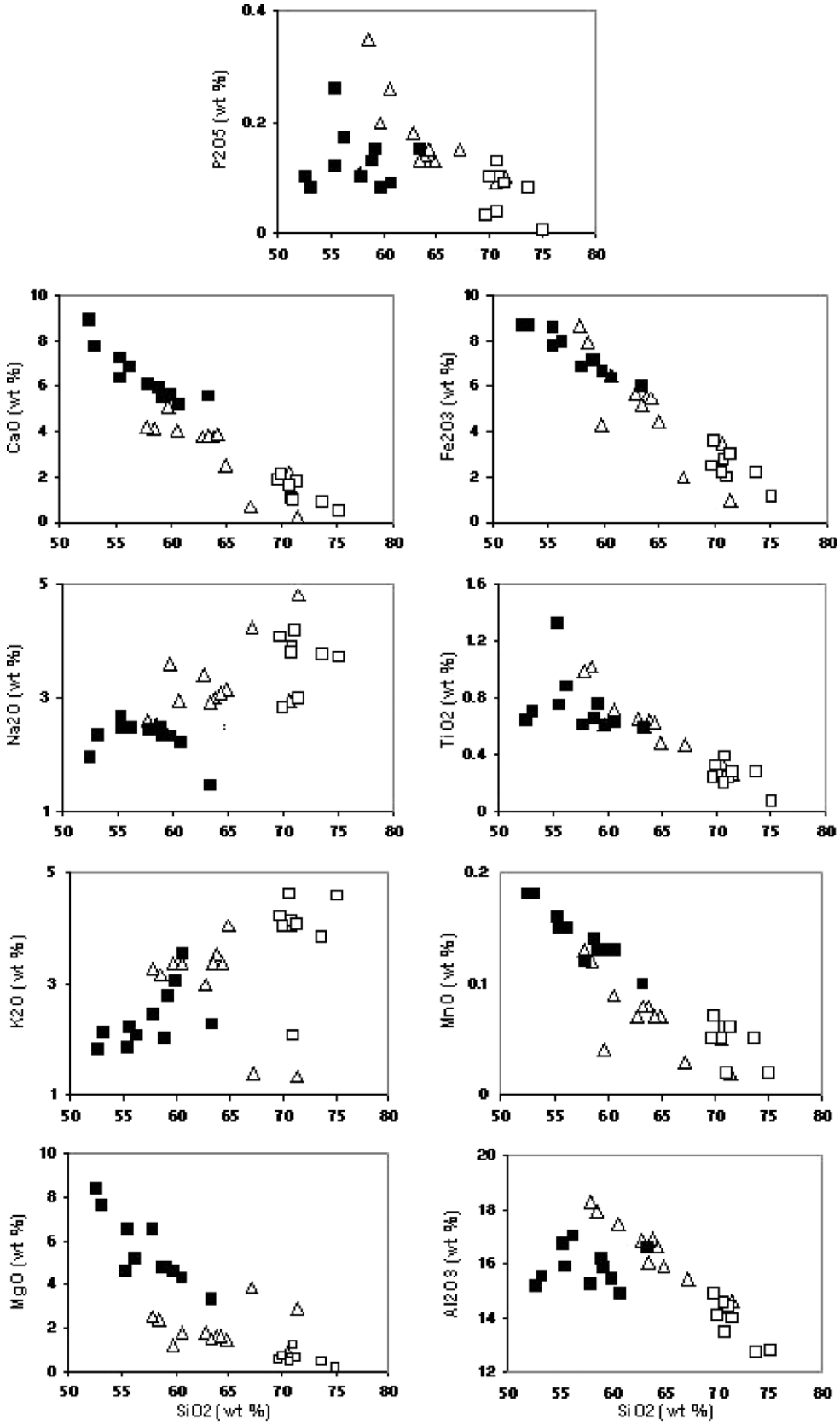

Fig. 6. Harker diagrams for major elements of the Boroujerd Granitoid Complex. Symbols: ■ quartz-dioritic unit, □: monzogranitic unit, △: granodioritic unit.

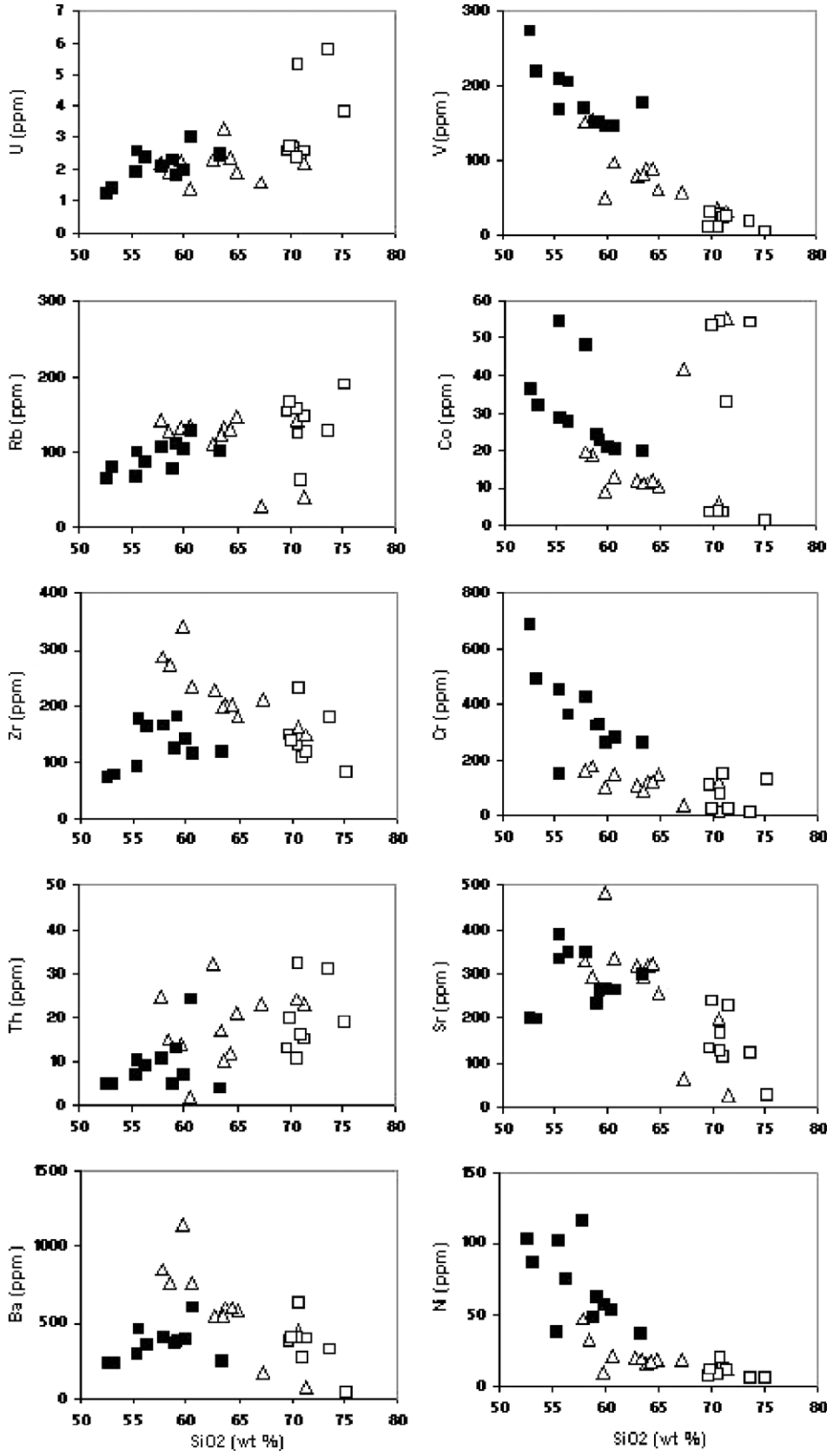

Fig. 7. Harker diagrams for selected trace elements of the Boroujerd Granitoid Complex. Symbols as in Fig. 6.

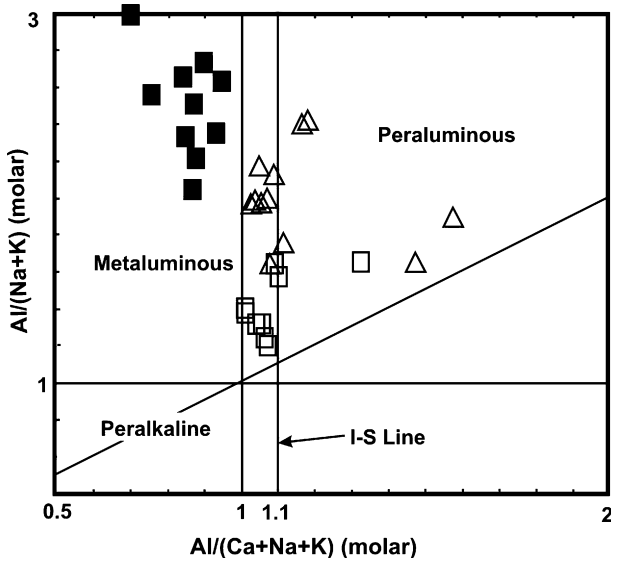

Fig. 8. Molar A/CNK [$Al_2O_3/(CaO + Na_2O + K_2O)$] vs. A/NK [$(Al_2O_3)/(Na_2O + K_2O)$] diagram (Shand, 1947) for the Boroujerd Granitoid Complex. Symbols as in Fig. 6.

different magmatic processes. In the $Al_2O_3/(CaO + Na_2O + K_2O)$ versus $Al_2O_3/(Na_2O + K_2O)$ [A/CNK vs. A/NK] diagram (Shand, 1947) (Fig. 8); the composition of quartz-dioritic unit plots in the metaluminous field, while the granodioritic and monzogranitic unit plot into the peraluminous domain. Nevertheless, the ratio of the molecular A/CNK of the quartz-dioritic unit as well as most of the granodioritic and monzogranitic units are in the 1–1.1 interval of A/CNK (Fig. 8), hence the rocks are of I-type in the sense of Chappell and White (1974). On the basis of the Irvine and Baragar (1971) classification scheme (Fig. 9a) all samples belong to the calc-alkaline series, and fall in the high to medium-K calc-alkaline field in the K_2O vs. SiO_2 diagram of Rickwood (1989) (Fig. 9b). Some of the samples (MA3, GM5 and AB6) fall in the medium-K calc-alkaline field and their K_2O contents are inconsistent with their silica contents, which could be due to some hydrothermal alteration.

4.3. Trace elements

Trace element contents are presented in Table 3 and their variations versus SiO_2 are plotted in Harker diagrams (Fig. 7). As was observed for the major elements, the quartz-diorite unit defines a distinct domain in the trace element diagrams, clearly shown by the Cr, Rb and Zr variations, suggesting a different source (or magmatic processes) for that unit. The transition elements (Ni, Cr, Co, V) display a pronounced negative correlation with their silica content, that is, they behave as compatible elements. The decrease of the V content with increasing SiO_2 is evidence for the fractionation of Fe–Ti oxides. The Sr and Zn variations show a negative trend, whereas Rb, U, Ta, Nb and Th show a positive correlation and Hf, Zr, Yb, Y, Nd, Ga, Ce and La are scattered, in comparison with the other elements (Table 3; Fig. 7). The high-field strength elements (Nb, Ta and Hf) are generally low. The Nb content is lower than the average value of felsic I-type granites (20 ppm), but is in the range of I-type (14 ppm) granites in the Lachlan Belt of southeastern Australia (Chappell and White, 1992). Sr contents in fresh samples range from 484 to 66 in the granodioritic unit, from 388 to 197 ppm in the quartz-diorite unit and from 269 to 114 ppm in the monzogranitic unit. This element behaves as a compatible element, suggesting the role of plagioclase fractionation in the formation of these rocks. Ba contents range from 1150 to 172 ppm in the granodioritic unit, from 596 to 236 ppm in the quartz-dioritic unit, and from 631 to 38 ppm in the monzogranitic unit. This element behaves as an incompatible element in the quartz-diorites but is compatible in the other units.

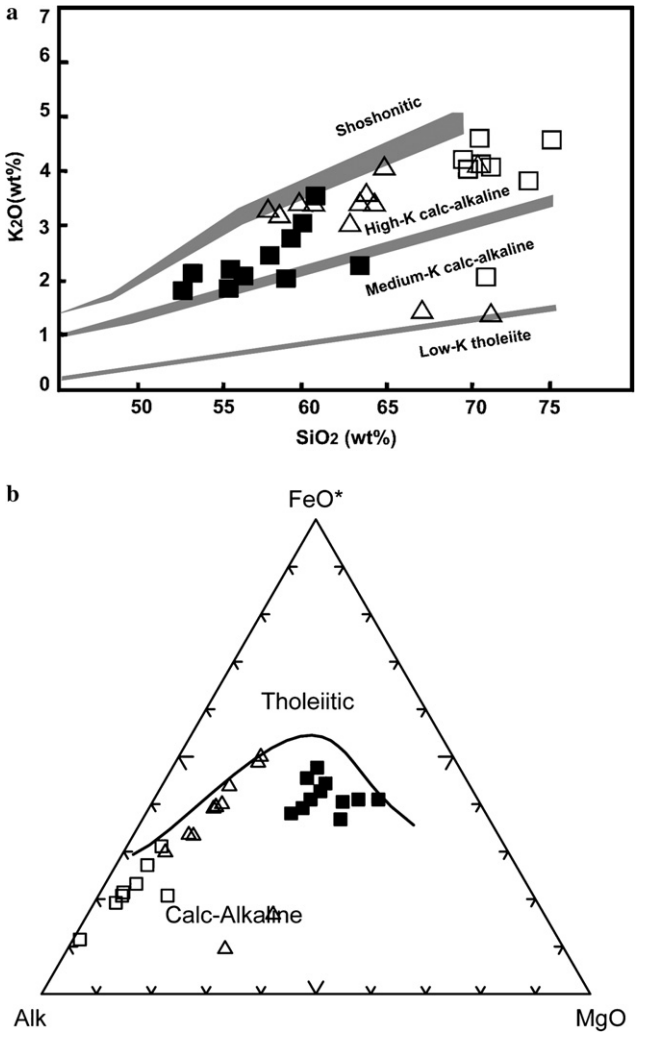

Fig. 9. (a) K_2O vs. SiO_2 diagrams with field after Rickwood (1989); (b) AFM diagram with field delineated after Irvine and Baragar (1971). Symbols as in Fig. 6.

Trace element distribution patterns for the granodioritic, quartz-dioritic and monzogranitic units from the Boroujerd Complex are normalized to chondrites in Fig. 10 following Thompson (1982). All the studied samples show

Ta, Nb, Ti, P and Sr depletion and are enriched in LILE (Rb, K, and Th). In comparison with HFSE (Nb, Ta, Hf, Zr, Sm, Y, and Yb), the LREE (La, Ce, Nd) show enrichment. High Rb, Th, K and low Sr, P and Ti values are compatible with typical crustal melts (Harris et al., 1986; Chappell and White, 1992) and suggest some upper crustal contamination during magmatic evolution. Another explanation is that they display the signature of a subduction component, i.e. fluids (or melts) derived from the subducted sediments. The Nb–Ta trough is typical for calk-alkaline magmas formed above a subduction zone.

Chondrite-normalized REE (Rare Earth Elements) patterns are shown in Fig. 11 using the chondrite-normalized values of Nakamura (1974). The light REE (LREE) patterns show enrichment as 90–120 times chondrite for the granodioritic unit, 40–100 times for the quartz-dioritic unit and 60–110 times for the monzogranitic unit. The samples of the granodioritic unit exhibit strongly fractionated REE

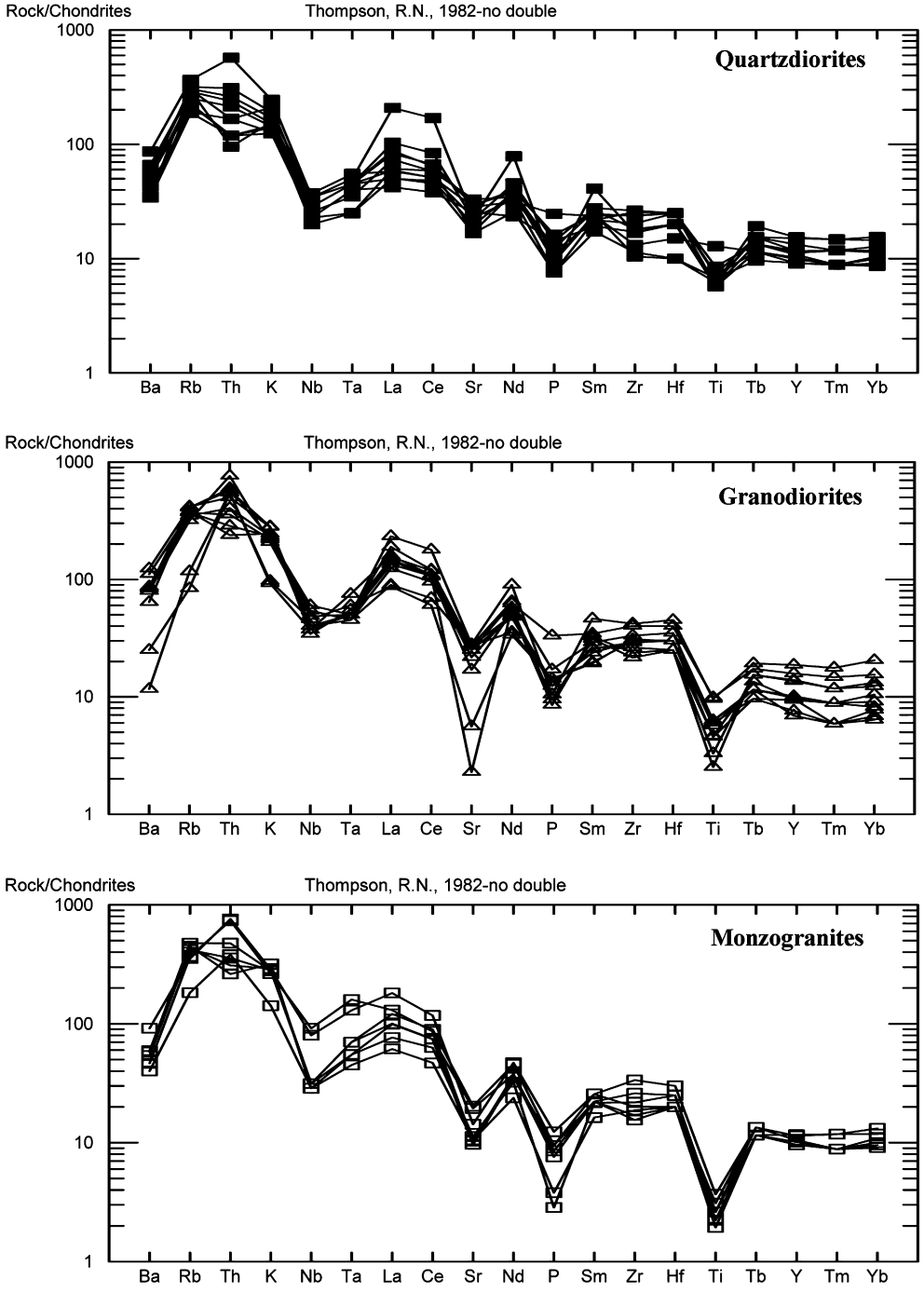

Fig. 10. Chondrite-normalised, trace element abundance diagrams (spider diagrams) for representative samples of the studied granitoid complex. Normalization factors are from Thompson (1982). Symbols as in Fig. 6.

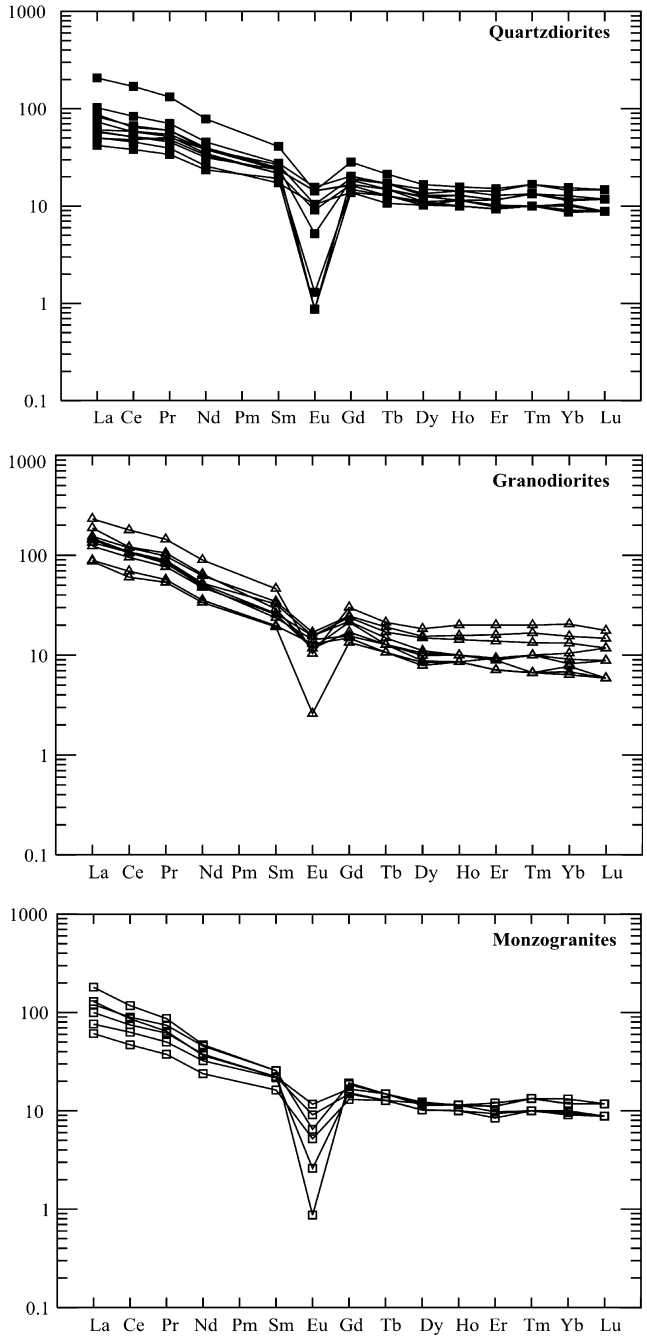

Fig. 11. Chondrite-normalized REE patterns (values from Nakamura, 1974). Symbols as in Fig. 6.

patterns ($[La/Yb]_N = 10–53$), in which variable Eu anomalies ($Eu/Eu^* = 0.2–1.1$) and flat heavy REE (HREE) patterns are visible. The samples of the quartz-diorite unit again show strong fractionated REE patterns ($[La/Yb]_N = 3–13$), but flatter heavy REE patterns with moderate negative Eu anomalies ($Eu/Eu^* = 0–0.7$). The samples of the monzogranitic unit are characterized by strongly fractionated and flatter heavy REE patterns than granodiorites ($[La/Yb]_N = 5–15$) and have strong to moderate negative Eu anomalies ($Eu/Eu^* = 0–0.6$).

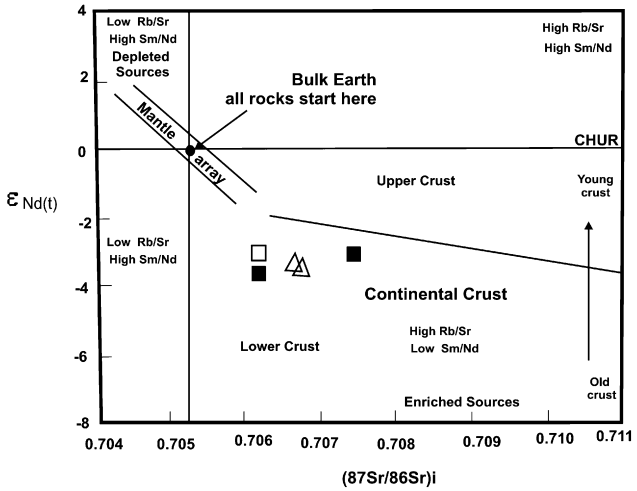

Fig. 12. Initial εNd_t values vs. initial Sr isotopic ratios. Symbols as in Fig. 6.

4.4. Isotopes

Five samples (2 from the granodioritic unit, 2 from quartz-dioritic unit and 1 from monzogranitic unit) were selected for determination of $^{143}Nd/^{144}Nd$ and $^{87}Sr/^{86}Sr$ isotopic ratios, corrected to the 170 Ma age of the Boroujerd granitoids. The results are presented in Table 4. All the samples plot in the lower right quadrangle of the Sr–Nd diagram corresponding to lower crustal signatures (Fig. 12). All of these samples are characterized by low negative ε_{Nd} values (between −3.02 and −3.62) and plot close together, a feature which shows a genetic link between the different rock types.

Low negative ε_{Nd} values may suggest a metaigneous protoliths of lower crust for the quartz-dioritic, granodioritic and monzogranitic units. Similarly, the $^{87}Sr/^{86}Sr$ initial isotopic ratios of the granodioritic and monzogranitic unit are close together (between 0.7063 and 0.7066), but show some higher values (between 0.7062 and 0.7074) for the quartz-dioritic unit. This could also indicate different magmatic processes and/or different crustal protoliths having dissimilar compositions in a deforming active margin for these rocks.

5. Discussion

5.1. Tectonic setting and geotectonic model

The Boroujerd Granitoid Complex is formed of a high-K calc-alkaline suite (Fig. 9b), in which quartz-diorite, granodiorite and monzogranite are the dominant rock types. In respect of their field relations (see Section 1), petrography (see Section 3) and geochemistry (see Section 4) these rocks show similarity to intrusions of active continental margins. Numerous studies suggest that trace elements can be used to discriminate between the different tectonic settings of granitoid magmas (e. g. Pearce, 1983;

Pearce et al., 1984; Harris et al., 1986), although they must be used with caution, as they could represent the formation of the protoliths, rather than those of the derived magma. The Boroujerd granitoids in the geotectonic classification of Pearce et al. (1984) are classified as volcanic arc granites (Fig. 13). Furthermore, as discussed earlier (Section 4.3), granitoids of the Boroujerd area are enriched in LILE such as Cs, K, Rb, and Th with respect to the HFSE, especially Nb and Ti (Fig. 10). Magmas with these geochemical characters are generally ascribed to subduction-related environments (e.g. Rogers and Hawkesworth, 1989; Sajona et al., 1996). High Th/Yb ratios correlated with high values for La/Yb are consistent with continental arc magmas (Fig. 14).

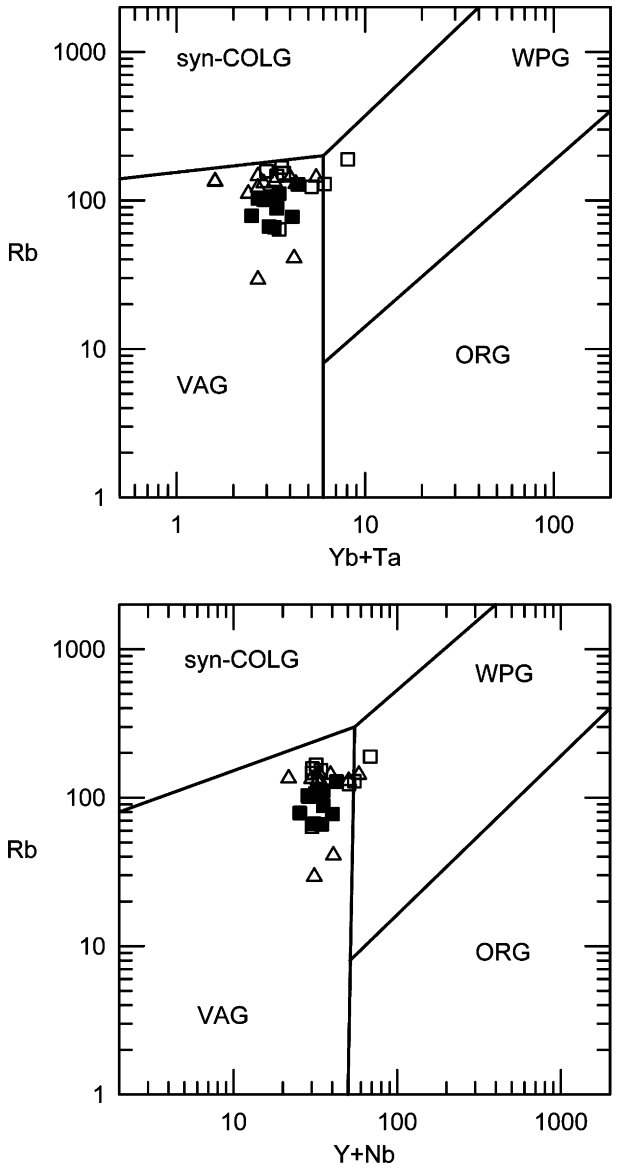

Fig. 13. Rb vs. (Nb + Y) and Rb vs. (Y + Nb) diagrams of Pearce et al. (1984); ORG, ocean-ridge granites; syn-COLG, syncollisional granites; VAG, volcanic arc granites; WPG, within-plate granites. Symbols as in Fig. 6.

5.2. Petrogenetic considerations and origin of the parent magmas

The quartz-dioritic samples and the most of the granodioritic and monzogranitic samples from the Boroujerd granitoids belong to the I-type granites of Chappell and White (1974). The S-type affinity shown by a few samples of the granodioritic and monzogranitic units may also represent highly fractionated I-type granites, as these rocks commonly reach and even slightly exceed aluminium saturation (Chauris, 1991; Chappell, 1999), or may be due to contamination by reaction with country rocks.

Regarding the origin of felsic arc magmas, two petrogenetic models have been proposed by different researchers. According to the first model felsic arc magmas are derived from basaltic parent magmas by Assimilation and Fractional Crystallization (AFC) processes (e.g. Grove and Donnelly-Nolan, 1986; Bacon and Druitt, 1988) and Melting, Assimilation, Storage and Homogenisation (MASH) processes (Hildreth and Moorbath, 1988). The MASH model applies to entire magma generation. Mantle and crustal magmas mixing close to the mantle-crust boundary, establish the characteristic chemical signature of magmas at the melting stage. The age and consequent chemical composition of the lower crustal component controls the isotopic variations during the assimilation stage. Finally, AFC processes may substantially modify the composition of the ascending magmas, resulting in the homogenisation stage (Hildreth and Moorbath, 1988).

In the second model, basaltic magmas provide heat for the partial melting of crustal rocks (e.g. Bullen and Clynne, 1990; Roberts and Clemens, 1993; Tepper et al., 1993; Guffanti et al., 1996). The mantle is also the heat source that controls crustal melting (Vigneresse, 2004). Other mechanisms for crustal melting require either advective or diffusive heat. Heat transfer by the former process brings hot material from the mantle and rapidly heats up the crust (Vigneresse, 2004).

The low concentration of the transitional elements (Ni, Cr, Co, V), the large volume of the granitoid rocks and the absence of rocks with basaltic compositions (all samples have SiO_2 content >52%, Table 3) in the Boroujerd area, suggest that it is unlikely that the voluminous felsic magmas were generated by differentiation of a mantle-derived mafic basaltic parent magma. It seems also unlikely that these granitoids represent mixtures of basaltic and granitic magmas, as evidence of mixing (e.g. coeval basaltic members) are lacking in the Boroujerd area. In addition, the Boroujerd granitoids are high-K, I-type, calc-alkaline rocks, characterized by pronounced negative Ba, Sr, Nb, Ta, P and Ti anomalies, enriched in Rb, Th, K, Ce, La and Nd, and have $\varepsilon Nd\ (t)$ values of −3.62 to −3.02, and $^{87}Sr/^{86}Sr$ initial isotopic ratios of 0.7062–0.7074. A crustal source of the granitoids is also indicated by the Sr–Nd isotopes (Fig. 12). The abundance of incompatible elements (K, Th, U, Rb, La, Ce) and the negative Eu anomaly support an intra-crustal origin for the granitoids of the Borou-

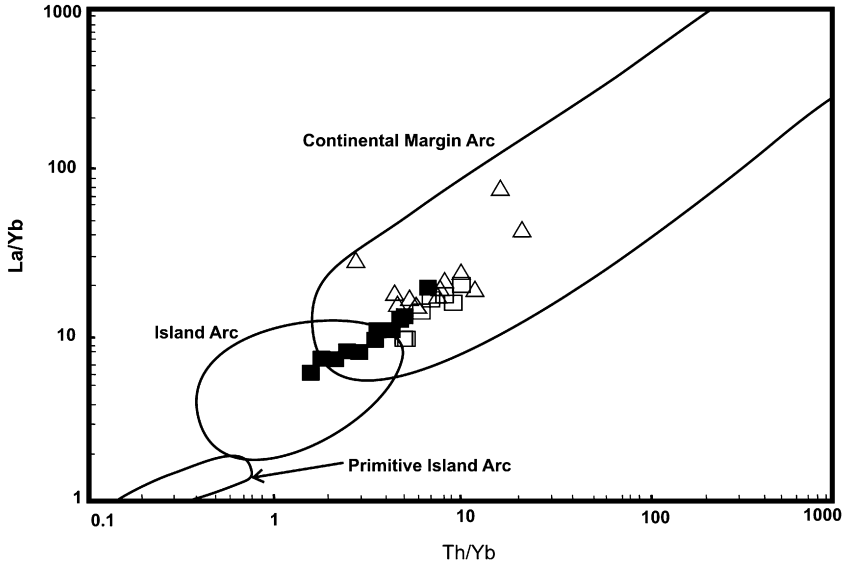

Fig. 14. La/Yb vs. Th/Yb diagram after Condie (1989). Symbols as in Fig. 6.

jerd area. In conclusion, it could be suggested that the Boroujered granitoids originated by partial melting of crustal protoliths having different compositions in a deforming active margin. In such a setting, mantle melts emplaced into the lower crust, were the most likely supplier of the heat required for crustal anatexis.

Fractional crystallization of the melts en route to higher crustal levels can generate the whole spectrum of granitoid types represent in the Boroujerd area. Increases in Na_2O, K_2O and decreases in TiO_2, Fe_2O_3, CaO, MgO, MnO, P_2O_5 and Al_2O_3 contents shown in the granitoids are compatible with their evolution through fractional crystallization processes (Fig. 6). Negative Ba and Sr anomalies in rocks from the Boroujerd area are associated with negative Eu anomalies, indicating evolution by fractionation of K-feldspar and plagioclase, either in magma chambers or during magma ascent. This is also supported by negative correlations between CaO, Al_2O_3, and SiO_2 (Fig. 6). The fractionation of plagioclase has played an important role in the petrogenesis of the Boroujerd granitoids, as indicated by significant anomalies of Eu, Ba, and Sr (Figs. 10 and 11). Decreases in P_2O_5 with increasing SiO_2 content are attributed to fractionation of apatite (Fig. 6). The unfractionated HREE (and Y) patterns (Fig. 10) suggest that the magma was produced outside the garnet stability field whereas the negative Eu and Sr anomalies (Figs. 10 and 11) could indicate that plagioclase was stable in the source.

6. Conclusions

The Boroujerd Granitoid Complex is made of three almost synchronous units (169–170 Ma) including granodioritic, quartz-dioritic and monzogranitic units. The geochemical characteristics, mineralogy and petrography of these units are comparable with typical I-type granites. The complex belongs to metaluminous to a slightly peraluminous, high-K calc-alkaline series, and displays geochemical characteristics typical of volcanic arc granites related to an active continental margin. The Sr–Nd isotope data for the Boroujerd granitoids are consistent with derivation from a crustal source and it could be suggested that the granitoids originated by partial melting of crustal protoliths having different compositions in a deforming active margin. This conclusion is in good agreement with the general model of Berberian (1983) and Shahabpour (2005), who proposed that the Sanandaj-Sirjan calc-alkaline magmatic arc formed over a high angle subducting oceanic slab in a Neotethyan subduction zone during Late Triassic to Late Cretaceous time.

Acknowledgments

This work was supported by Grant No 83066 from I.R.Iran National Science Foundation received by Dr. D. Esmaeily and Grant no 6105013/1/01 from the University of Tehran of I.R. Iran, received by M.V. Valizadeh. M. Berberian is thanked for his invaluable comments and suggestions. J. Ramezani (MIT, USA) is also thanked for his assistance in determination of Sr and Nd isotopic ratios and the U–Pb single zircon dating. Constructive reviews by Prof. A. Nédélec (University of Paul-Sabatier, Toulouse, France), Dr. Michael Crow and Dr. John Cobbing (both from British Geological Survey, UK) are warmly acknowledged.

References

Agard, P., Omrani, J., Jolivet, L., Mouthereau, F., 2005. Convergence history across Zagros (Iran): constraints from collisional and earlier deformation. International Journal of Earth Sciences (Geologische Rundschau) 94, 401–419.

Ahmadi Khalaji, A., 2006. Petrology of the granitoid rocks of the Boroujerd area. Ph.D Thesis, University of Tehran, Tehran, Islamic Republic of Iran.

Ahmadi Khalaji, A., Ghaderi, M., Ramezani, J., Valizadeh, M.V., 2005. U–Pb geochronology of the Jurassic Boroujerd plutonic Complex and associated intrusions within the Sanandaj-Sirjan Zone. Journal of Sciences, Islamic Republic of Iran. (in press).

Alavi, M., 1994. Tectonic of the Zagros orogenic belt of Iran: new data and interpretations. Tectonophysics 229, 211–238.

Bacon, C.R., Druitt, T.H., 1988. Compositional evolution of the zoned calc-alkaline magma chamber of Mt. Mazama, Crater Lake, Oregon. Contributions to Mineralogy and Petrology 98, 224–256.

Bechennec, F., Le Metour, J., Rabu, D., Bourdillon-de-Grissac, Ch., De Weaver, P., Beurrier, M., Villey, M., 1990. The Hawasina Nappes: stratigraphy, palaeogeography and structural evolution of a fragment of the south-Tethyan passive continental margin. In: Robertson, R.H.F., Searle, M.P., Ries, A.C. (Eds.), The Geology and Tectonics of the Oman Region, Geological Society of London. Special Publication, 49, pp. 213–223.

Berberian, M., 1977. Three phases of metamorphism in Haji-Abad quadrangle (southern extremity of the Sanandaj-Sirjan structural Zone): a palaeotectonic discussion. In: Berberian, M. (Ed.). Geological Survey of Iran, Report 40, Tehran, Iran, pp. 239–263.

Berberian, M., 1981a. The South Caspian: a compressional depression floored by a trapped, modified oceanic crust. Canadian Journal of Earth Sciences 20, 163–183.

Berberian, M., 1981b. Generalized Tectonic Map of Iran. Geological Survey of Iran 1, 6,450,00.

Berberian, M., 1983. Generalized tectonic map of Iran. In: Berberian, M. (Ed.). Continental Deformation in the Iranian Plateau. Geological Survey of Iran, Report No. 52.

Berberian, F., Berberian, M., 1981. Tectono-plutonic episodes in Iran. In: Gupta, H.K., Delany, F.M. (Eds.), Zagros Hindukush, Himalaya Geodynamic Evolution. American Geophysical Union, Washington, DC, pp. 5–32.

Berberian, M., King, G.C.P., 1981. Towards a paleogeography and tectonic evolution of Iran. Canadian Journal of Earth Sciences 18, 210–265.

Berberian, F., Muir, I.D., Pankhurst, R.J., Berberian, M., 1982. Late Cretaceous and early Miocene Andean type plutonic activity in northern Makran and central Iran. Journal of Geological Society of London 139, 605–614.

Berthier, F., Billiaul, H.P., Halbroronn, B., Marizot, p., 1974. Etude Stratigraphique, petrologique et structural de la région de Khorramabad (Zagros, Iran). Thése de 3e cycle, Grenoble, pp. 282.

Besse, J., Torcq, F., Gallet, Y., Ricou, L.E., Krystyn, L., Saidi, A., 1998. Late Permian to Late Triassic palaeomagnetic data from Iran: constraints on the migration of the Iranian block through the Tethyan Ocean and initial destruction of Pangaea. Geophysical Journal International 135, 77–92.

Bullen, T.D., Clynne, M.A., 1990. Trace element and isotopic constraints on magmatic evolution at Lassen volcanic center. Journal of Geophysical Research 95, 19671–19691.

Chappell, B.W., 1999. Aluminium saturation in I- and S-type granites and the characterization of fractionated haplogranites. Lithos 46, 535–551.

Chappell, B.W., White, A.J.R., 1974. Two contrasting granite types. Pacific Geology 8, 173–174.

Chappell, B.W., White, A.J.R., 1992. I and S-type granites in the Lachlan Fold Belt. Transactions of the Royal Society of Edinburgh: Earth Sciences 83, 1–26.

Chauris, L., 1991. Le granite à tourmaline de Plouarzel (Finistere): aspects chimico-mineralogiques d'une differenciation marginale leocogranitique. Géologie de la France 4, 31–38.

Condie, K.C., 1989. Geochemical changes in basalts and andesites across the Archean–Proterozoic boundary: identification and significance. Lithos 23, 1–18.

Cotten, J., Le Dez, A., Bau, M., Caroff, M., Maury, R.C., Dulski, P., Fourcade, S., Bohn, M., Brousse, R., 1995. Origin of anomalous rare earth element and yttrium enrichment in subaerially exposed basalts: evidence from France Polynesia. Chemical Geology 119, 115–138.

Davoudzadeh, M., Schmidt, K., 1984. A review of the Mesozoic paleogeography and paleotectonic evolution of Iran. Neues Jahrbuch für Geologie und Palaeontologie, Abhandlungen 168, 182–207.

Dercourt, J., Zonenshain, L.P., Ricou, L.E., Kazmin, V.G., Le Pichon, X., Knipper, A.L., Grandjacquet, C., Sbortshikov, I.M., Geyssany, J., Lepverier, C., Pechersky, D.H., Boulin, J., Sibuet, J.C., Savostin, L.A., Sorokhtin, O., Westphal, M., Bazhenov, M.L., Lauer, L.P., Biju-Duval, B., 1986. Geological evolution of the Tethys belt from the Atlantic to the Pamirs since the Lias. Tectonophysics 123, 241–315.

Farhoudi, G., 1978. A comparison of Zagros geology to island arcs. Journal of Geology 86, 323–334.

Grove, T.L., Donnelly-Nolan, J.M., 1986. The evolution of young silicic lavas at Medicine Lake Volcano, California: implications for the origin of compositional gaps in calc-alkaline series lavas. Contribution to Mineralogy and Petrology 92, 281–302.

Guffanti, M., Clynne, M.A., Muffler, L.J.P., 1996. Thermal and mass implications of magmatic evolution in the Lassen volcanic region, California, and constraints on basalt influx to the lower crust. Journal of Geophysical Research 101, 3001–3013.

Hacker, B.R., Mosenfelder, J.L., Gnos, E., 1996. Rapid emplacement of the Oman ophiolite: thermal and geochronologic constraints. Tectonics 15, 1230–1247.

Harris, N.B.W., Pearce, J.A., Tindle, A.G., 1986. Geochemical characteristics of collision-zone magmatism. In: Coward, M.P., Ries, A.C. (Eds.), Collision Tectonics. Geological Society London, Special Publication 19, pp. 67–81.

Hildreth, E.W., Moorbath, S., 1988. Crustal contributions to arc magmatism in the Andes of Central Chile. Contributions to Mineralogy and Petrology 76, 177–195.

Hooper, R.J., Baron, I., Hatcher Jr., R.D., Agah, S., 1994. The development of the southern Tethyan margin in Iran after the break up of Gondwana: implications of the Zagros hydrocarbon province. Geosciences 4, 72–85.

Immenhauser, A., Schreurs, G., Gnos, E., Oterdoom, H.W., Hartmann, B., 2000. Late Palaeozoic to Neogene dynamic evolution of the northeastern Oman margin. Geological Magazine 137, 1–18.

Irvine, T.N., Baragar, W.R.A., 1971. A guide to the chemical classification of the common volcanic rocks. Canadian Journal of Earth Sciences 8, 523–548.

Jankovic, S., 1984. Metallogeny of the Alpine granitoids in the Tethyan–Eurasian metallogenic belt. Proceedings of the 27th International Geological Congress, Moscow, 4–14 August, 1984, 247–274.

Knipper, A.L., Ricou, L.E., Dercourt, J., 1986. Ophiolites as indicators of the geodynamic evolution of the Tethyan ocean. Tectonophysics 123, 213–240.

Masoudi, F., 1997. Contact metamorphism and pegmatite development in the SW of Arak, Iran. PhD thesis, The University of Leeds, UK, pp. 231.

Masoudi, F., Yardley, B.W.D., Cliff, R.A., 2002. Rb-Sr geochronology of pegmatites, plutonic rocks and a hornfels in the region southwest of Arak, Iran. Islamic Republic of Iran Journal of Sciences 13 (3), 249–254.

Mohajjel, M., 1997. Structure and tectonic evolution of Palaeozoic–Mesozoic rocks, Sanandaj–Sirjan Zone, western Iran. Ph.D. Thesis, University of Wollongong, Wollongong, Australia.

Mohajjel, M., Fergusson, C.L., 2000. Dextral transpression in Late Cretaceous continental collision, Sanandaj–Sirjan Zone, Western Iran. Journal of Structural Geology 22, 1125–1139.

Mohajjel, M., Fergusson, C.L., Sahandi, M.R., 2003. Cretaceous–Tertiary convergence and continental collision, Sanandaj-Sirjan Zone, Western Iran. Journal of Asian Earth Sciences 21, 397–412.

Nakamura, N., 1974. Determination of REE, Ba, Fe, Mg, Na, and K in carbonaceous and ordinary chondrites. Geochimica et Cosmochimica Acta 38, 757–775.

Pearce, J.A., 1983. Role of the sub-continental lithosphere in magma genesis at active continental margins. In: Hawkesworth, C.J., Norry, M.J. (Eds.), Continental Basalts and Mantle Xenoliths. Shiva Publishing, Nantwich, pp. 158–185.

Pearce, J.A., Harris, N.B.W., Tindle, A.G., 1984. Trace element discrimination diagrams for the tectonic interpretation of granitic rocks. Journal of Petrology 25, 956–983.

Rickwood, P.C., 1989. Boundary lines within petrologic diagrams which use of major and minor elements. Lithos 22, 247–263.

Ricou, L.E., 1994. Tethys reconstructed: plates, continental fragments and their boundaries since 260 Ma from Central America to South-eastern Asia. Geodinamica Acta (Paris) 7 (4), 169–218.

Ricou, L.E., Braud, J., Brunn, J.A., 1977. Le Zagros. Mémoire Societe Géologique de France 8, 33–52.

Roberts, M.P., Clemens, J.D., 1993. Origin of high-potassium, calc-alkaline, I-type granitoids. Geology 21, 825–828.

Rogers, G., Hawkesworth, C.J., 1989. A geochemical traverse across the North Chilean Andes: evidence for crust generation from the mantle wedge. Earth and Planetary Science Letters 91, 271–285.

Sabzehei, M., 1994. Geological Quadrangle Map of Iran, No. 12, Hajiabad, 1:250,000, First compilation by Berberian, M., final compilation and revision by Sabzehei, M., Geological Survey of Iran.

Saidi, A., Brunet, M.F., Ricou, L.E., 1997. Continental accretion of the Iran block to Eurasia as seen from late Paleozoic to early Cretaceous subsidence curves. Geodinamica Acta 10, 189–208.

Sajona, F.G., Maury, R.C., Bellon, H., Cotton, J., Defant, M., 1996. High field strength elements of Pliocene-Pleistocene island-arc basalts Zamboanga Peninsula, Western Mindanao (Philippines). Journal of Petrology 37, 693–726.

Sengör, A.M.C., 1984. The Cimmeride Orogenic System and the Tectonics of Eurasia, Geological Society of America Special Paper, 195p.

Sengör, A.M.C., 1990. A new model for the late Paleozoic–Mesooic tectonic evolution of Iran and implications for Oman. In: Robertson, A.H.F., Searle, M.P., Ries, A.C. (Eds.). the Geology and Tectonics of the Oman Region, Geological Society of London, Special Publication, 22, pp. 278–281.

Sengör, A.M.C., 1991. Late Paleozoic and Mesozoic evolution of the Middle Eastern Tethysides: Implications for the Paleozoic Geodynamics of the Tethyan Realm. IGCP Project 276, Newsletter No. 2, pp. III-149.

Sengör, A.M.C., Altmer, D., Cin, A., Ustaomer, T., Hsu, K.J., 1988. Origin and assembly of the Tethyside orogenic collage at the expense of Gondwana Land. In: Audley-Charles, M.G., Hallam, A., Editors, 1988. Gondwana and Tethys, Geological Society of London, Special Publication 37, pp. 119–181.

Sengör, A.M.C., Natal'in, B.A., 1996. Paleotectonics of Asia: fragments of the synthesis. In: Yin, A., Harrison, T.M. (Eds.), The Tectonic Evolution of Asia. Cambridge University Press, Cambridge, pp. 486–640.

Shahabpour, J., 1994. Post-mineralization breccia dike from the Sar Cheshmeh porphyry copper porphyry system, Kerman, Iran. Exploration and Mining Geology 3, 39–43.

Shahabpour, J., 2005. Tectonic evolution of the orogenic belt in the region located between Kerman and Neyriz. Journal of Asian Earth Sciences 24, 405–417.

Shahabpour, J., Kramers, J.D., 1987. Lead isotope data from the Sar Cheshmeh Porphyry copper deposit, Kerman, I.R. Iran. Mineralium Deposita 22, 278–281.

Shand, S.J., 1947. Eruptive Rocks. D. Van Nostrand Company, New York, 360p.

Sohieili, M., 1992. Geological quadrangle map of the Khorramabad area, No: D 7. 1: 250 000, Geological Survey of Iran, Tehran, Iran.

Stöcklin, J., 1968. Structural history and tectonics of Iran; a review. American Association of Petroleum Geologists Bulletin 52, 1229–1285.

Stöcklin, J., 1974. Possible ancient continental margins in Iran. In: Burk, C.A., Drake, C.L. (Eds.), The Geology of Continental Margins. Springer, Berlin, pp. 873–887.

Stöcklin, J., 1977. Structural correlation of the Alpine range between Iran and Central Asia. Mémoire Hors-Sérve No. 8 de la Sociètè Géologique de France 8, 333–353.

Stöcklin, J., Setudinia, A., 1972. Lexique Stratigraphique International Volume III ASIE. Centre National de la Récherche Scientifique. 15, quai Anatole-France 75p. (Paris-VII).

Takin, M., 1972. Iranian geology and continental drift in the Middle East. Nature 235, 147–150.

Tepper, J.H., Nelson, B.K., Bergantz, G.W., Irving, A.J., 1993. Petrology of the Chilliwack Batholith, North Cascades, Washington: generation of calc-alkaline granitoids by melting of mafic lower crust with variable water fugacity. Contributions to Mineralogy and Petrology 113, 333–351.

Thompson, A.B., 1982. Magmatism of the British Tertiary Volcanic Province. Scottish Journal of Geology 18, 49–107.

Tronnes, R.G., Brandon, A.D., 1992. Mildly peraluminous high-silica granites in a continental rift: the Drammen and Finne Marka batholiths, Oslo Rift, Norway. Contributions to Mineralogy and Petrology 109, 257–294.

Vernant, P., Nilforoushan, F., Hatzfeld, D., Abbassi, M., Vigny, C., Masson, F., Nankali, H., Martinod, J., Ashtiani, A., Bayer, R., Tavakoli, F., Chéry, J., 2004. Contemporary crustal deformation and plate kinematics in Middle East constrained by GPS measurements in Iran and Northern Oman. Geophysical Journal International 157, 381–398.

Vigneresse, J.L., 2004. A new paradigm for granite generation. Transactions of the Royal Society of Edinburgh: Earth Sciences 95, 11–22.

Wasserburg, G.J., Jacobsen, S.B., Depalo, D.J., McCulloch, M.T., Wen, T., 1981. Precise determination of Sm/Nd ratios, Sm and Nd isotopic abundances in standard solutions. Geochimica et Cosmochimica Acta 45, 2311–2323.